

# Chapter 4

## Quantum scattering matrices

Chapters 2 and 3 have focused on the basic properties of the scattering matrices  $\underline{S}^{\text{LR}}$  and  $\underline{S}^{\text{core}}$ , and their relationship to the observables of an atom in external electric and/or magnetic fields. Simple formulas for both the bound state spectrum, Eq. (2.26), and the total photoabsorption cross section, Eq. (3.28), have been given in terms of these  $S$ -matrices. Clearly, for these results to be useful the  $S$ -matrices must be calculated. This chapter and the next give the details of how the long-range  $S$ -matrix  $\underline{S}^{\text{LR}}$  can be calculated using either a fully quantum mechanical approach (this chapter) or a semiclassical approximation similar to closed-orbit theory (Ch. 5).

At this point, it is worth reiterating an important point about the total photoabsorption cross section (3.28) derived in Ch. 3: it is an exact result that applies to any multichannel atom in any configuration of external electric and magnetic fields. This generality of my approach is one of its main strengths. However, to explore the physics contained in the photoabsorption cross section, it is useful to specialize to a narrower class of experiments. Consequently, the remainder of the thesis concentrates on the properties of a single channel atom in a static, external magnetic field. Once the  $S$ -matrices have been calculated for this system, the physics of the photoabsorption process can be studied.

For single channel atoms, such as the alkali-metal atoms, the core-region  $S$ -matrix is parametrized in terms of the quantum defects  $\mu_l$  [50]:

$$S_{ll'}^{\text{core}} = \delta_{ll'} e^{2\pi i \mu_l}.$$

This is a standard result from quantum-defect theory and the quantum defects for simple atoms are

available in many articles and books [96, 110]. While my formulation of the photoabsorption cross section applies to multichannel atoms, the physics of core-scattered peaks in recurrence spectra must be understood before these difficult cases can be treated. Single channel atoms provide an ideal setting to explore core scattering because all of the effects of the ionic core are parameterized by a few energy independent quantum defects. At this point, I only mention that for multichannel atoms the core-region  $S$ -matrix can be determined using well understood methods of quantum-defect theory,  $R$ -matrix theory and frame transformations [68]. These techniques are applicable immediately as the external fields are can be neglected in the core-region. Also note that quantum mechanical effects such as spin and the Pauli exclusion principle make semiclassical approximations more difficult for the core-region physics encapsulated in  $\underline{S}^{\text{core}}$ .

The long-range physics presents more of a challenge than the short range physics. The main difficulty is that in this region, the electronic Hamiltonian,

$$H = -\frac{1}{2}\nabla^2 - \frac{1}{r} + \frac{1}{2}B\hat{L}_z + \frac{1}{8}B^2\rho^2, \quad (4.1)$$

is nonseparable in two dimensions  $(\rho, z)$ . When an electron is highly excited, the two dimensional Schrödinger equation of Eq. (4.1) must be solved over a vast region of configuration space. More specifically, below the ionization threshold,  $\underline{S}^{\text{LR}}$  can be determined after the Schrödinger equation is solved in a spherical shell bounded by the radii  $r_0 < r < r_{max}$ . Typically  $r_0$  is somewhere in the matching region  $r_0 \approx 10 - 100$  a.u. (Ch. 2) and  $r_{max}$  is somewhere well beyond the classical turning point of the electron where the wavefunction has decayed to zero. A good estimate for the size of  $r_{max}$  is given by the formula,

$$r_{max} \approx 3\nu^2, \quad (4.2)$$

where  $\nu = 1/\sqrt{-2E}$  is the effective quantum number of the electron. As an example, for a  $\nu = 200$  electron, the outer radius  $r_{max}$  is an extraordinary 120,000 a.u. or  $\approx 6 \mu\text{m}$ . Besides the large region of space required and the two-dimensional, nonseparable Schrödinger equation that must be solved, there are two other difficulties in calculating  $\underline{S}^{\text{LR}}$ . First, because  $\underline{S}^{\text{LR}}$  is a strongly varying function of the energy, the Schrödinger equation must be solved at every energy at which the cross section is

desired. Second, because the preconvolved cross section requires  $\underline{S}^{\text{LR}}$  at complex energies  $E + i\Gamma/2$ , the solutions of the Schrödinger equation will be complex valued. This necessitates the costly use of complex arithmetic in the numerical implementation of the method.

While these difficulties slow computational efforts, no significant conceptual difficulties exist in carrying out the calculations of  $\underline{S}^{\text{LR}}$  at complex energies. In fact, a number of researchers have performed similar calculations [71, 76] for diamagnetic atoms using the time tested approach of  $R$ -matrix theory [111, 112, 113, 68]. My approach to calculating  $\underline{S}^{\text{LR}}$  follows this previous work with two differences. First, to obtain the preconvolved cross section directly from Eq. (3.28) variational  $R$ -matrix theory is extended to complex energies. Usually, the infinite resolution cross section is calculated with  $R$ -matrix calculations on the real energy axis, after which the convolved cross section is obtained by a numerical convolution. Because my preconvolved  $S$ -matrix approach for the cross section requires calculations at complex energies, it is generally slower at calculating the infinite resolution cross section than other approaches. However, the complex energy calculations described in this chapter have a distinct advantage in obtaining the convolved cross section. Second, my treatment is the first to package the solutions of the Schrödinger equation for the long-range region into an  $S$ -matrix. Most previous work has used  $R$ -matrices instead of  $S$ -matrices for this purpose. The main advantage of a long-range  $S$ -matrix is that all the interpretive tools of semiclassical approximations can be used to understand the physics contained in the  $S$ -matrix. This gives a simple picture of the quantum mechanics associated with the nonintegrable electronic motion. Interpretation of the long range  $R$ -matrix is far less transparent.

This chapter develops the necessary extensions of variational  $R$ -matrix theory needed to calculate  $\underline{S}^{\text{LR}}$  at complex energies for an atom in an external magnetic field. The basic ideas of  $R$ -matrix theory can be found in a number of articles so the more familiar parts of the theory will only be sketched. After the method for finding  $\underline{S}^{\text{LR}}$  has been described, calculations that implement this method are presented and discussed. The most important result of these calculations is that the physics contained in the exact quantum mechanical  $\underline{S}^{\text{LR}}$  can be extracted using the ideas of recurrence spectroscopy. Fourier transformation of  $\underline{S}^{\text{LR}}$  then permits an identification of the most important quantum mechanical paths of the electron as it scatters off the long-range fields.

## 4.1 Variational $S$ -matrix approach

Calculation of the long-range  $S$ -matrix involves two steps. The first is to solve the Schrödinger equation,

$$\hat{H}\psi(\vec{x}) = E\psi(\vec{x}), \quad (4.3)$$

in the long-range region for the Hamiltonian of Eq. (4.1). After numerical long-range solutions of Eq. (4.3) are obtained,  $\underline{S}^{\text{LR}}$  can be determined by a simple matching procedure. Both of these steps can be carried out using variational  $R$ -matrix theory. This technique has been developed [114, 115, 116] as an extension of the  $R$ -matrix theory of Wigner and Eisenbud [113]. In most situations, the Schrödinger equation (4.3) is solved (for a bound state) by imposing boundary conditions upon the wavefunction and then finding a discrete set of energy eigenvalues. In variational  $R$ -matrix theory this procedure is turned around: here, the **energy** is set beforehand and the Schrödinger equation is solved in a volume  $V$  to determine the **boundary conditions** of the wavefunction on the surface  $S$  of the volume. This information about the boundary conditions of wavefunction on the surface is encoded in the normal logarithmic derivative  $-b$  of the wavefunction on the surface:

$$-b = \frac{\partial\psi}{\partial n} \frac{1}{\psi}. \quad (4.4)$$

Here,  $\hat{n}$  denotes the outward unit vector normal to the surface. The main tool of variational  $R$ -matrix theory is a variational principle for this logarithmic derivative (4.4). This provides an efficient algorithm for finding the wavefunction  $\psi$  and its logarithmic derivative  $-b$  on a given surface  $S$ . In the following subsection, the details of this approach are sketched for the long-range motion of an atomic electron in an external magnetic field. After that, the long range  $S$ -matrix  $\underline{S}^{\text{LR}}$  is extracted from the results of the  $R$ -matrix calculation.

### 4.1.1 Solving the Schrödinger equation

The first step in  $R$ -matrix theory is to identify the volume  $V$  (and surface  $S$ ) over which the Schrödinger equation (4.3) must be solved. As mentioned before, for a calculation of  $\underline{S}^{\text{LR}}$ , a spherical

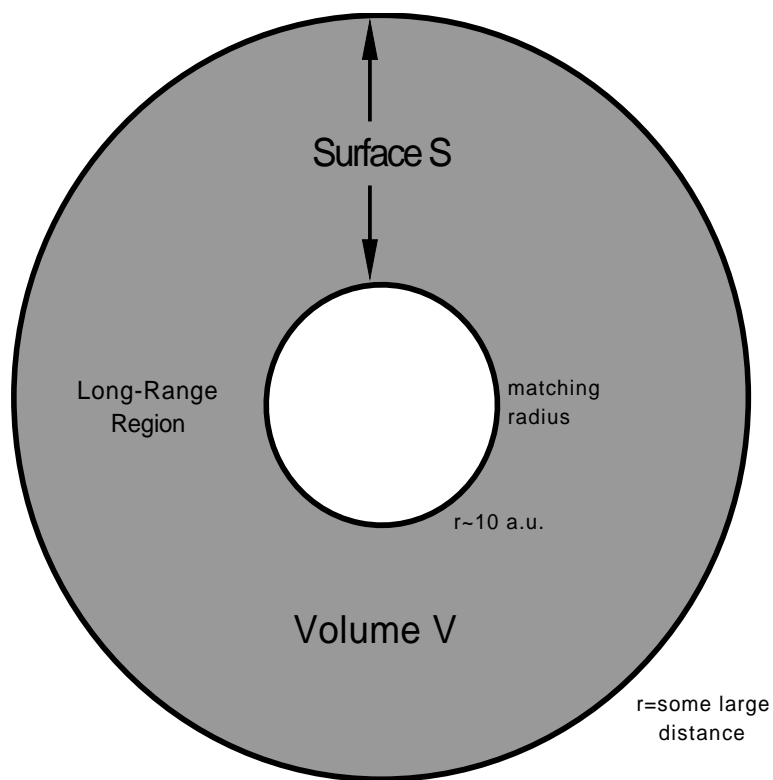


Figure 4.1: This diagram depicts the volume  $V$  of configuration space in which the Schrödinger equation must be solved to find the long-range  $S$ -matrix. The volume is bounded by the radii  $r_0$  and  $r_{max}$ , where  $r_0$  is somewhere in the matching region and  $r_{max}$  is a large distance beyond the classical turning point of the electron. The Hamiltonian in this volume, Eq. (4.1), involves both the Coulomb and diamagnetic potentials.

shell bounded by the radii  $r_0$  (in the matching region) and  $r_{max}$  (some large distance where the wavefunction has decayed to zero) is appropriate. The surface  $S$  of this volume has two parts: a sphere  $S_1$  at  $r = r_0$  having  $\hat{n} = -\hat{r}$  and a sphere  $S_2$  at  $r = r_{max}$  having  $\hat{n} = \hat{r}$ . This volume used in the  $R$ -matrix calculations for  $\underline{S}^{LR}$  is depicted in Fig. 4.1.

The standard formulas of variational  $R$ -matrix theory [68] apply to this case without major modifications. This technique begins with a variational principle, first derived by Kohn [117] and later by Greene [116], for the logarithmic derivative  $-b$  of the wavefunction  $\psi$  on the surface  $S$ ,

$$b = \frac{2 \int dV \psi^* (E - \hat{H}) \psi - \int dS \psi^* \frac{\partial \psi}{\partial n}}{\int dS |\psi|^2}. \quad (4.5)$$

As stated above, the energy  $E$  of the electron is a parameter in this equation and has a complex value of  $E + i\Gamma/2$  to accomplish the energy preconvolution of the cross section. Here and elsewhere, I use a flexible notation where at times  $E$  is the full complex valued energy (as in Eq. (4.5)) and at other times  $E$  is only the real part of the energy (implied in  $E + i\Gamma/2$ ). The context will determine which of these meanings is appropriate.

As is true of the Rayleigh-Ritz variational principle for the bound state energies of a Hamiltonian, the variational principle for  $b$  (4.5) can be converted to a generalized eigenvalue problem. This is done by expanding the  $\beta$ th linearly independent wavefunction  $\psi_\beta(\vec{x})$  in a set of  $N$  basis functions  $y_i(\vec{x})$  and undetermined coefficients  $c_{i\beta}$ :

$$\psi_\beta(\vec{x}) = \frac{1}{r} \sum_{i=1}^N y_i(\vec{x}) c_{i\beta}. \quad (4.6)$$

The resulting eigensystem,

$$\underline{\Gamma} \vec{c}_\beta = b_\beta \underline{\Lambda} \vec{c}_\beta, \quad (4.7)$$

is written in terms of the matrices

$$\Gamma_{ij} = 2 \int_V y_i^*(\vec{x}) (E - \hat{H}) y_j(\vec{x}) dV - \oint_S y_i^*(\vec{x}) \frac{\partial y_j(\vec{x})}{\partial n} dS \quad (4.8)$$

and

$$\Lambda_{ij} = \oint_S y_i^*(\vec{x}) y_j(\vec{x}) dS. \quad (4.9)$$

It is important not to confuse the matrix  $\underline{\Gamma}$  with the smoothing width  $\Gamma$ , which is always a scalar. As usual, the factor  $1/r$  is used in the wavefunction of Eq. (4.6) to eliminate the first derivatives  $\partial/\partial r$  in the Hamiltonian operator  $\hat{H}$  in Eq. (4.8). This explicit  $1/r$  factor in the wavefunction has three auxiliary effects on the above expressions. First, the infinitesimal volume element  $dV$  in Eq. (4.8) no longer has the usual  $r^2$  factor found in spherical polar coordinates, so that  $dV = dr d\theta d\phi \sin \theta$ . Second, the logarithmic derivative in Eq. (4.7) is defined with respect to  $r\psi_\beta$  rather than simply  $\psi_\beta$ :

$$-b_\beta = \frac{\partial(r\psi_\beta)}{\partial n} \frac{1}{r\psi_\beta}. \quad (4.10)$$

Third, the radial part of the kinetic energy operator in  $\hat{H}$  has the form  $-(1/2)d^2/dr^2$ . Solving the eigensystem of Eq. (4.7) yields the logarithmic derivative  $b_\beta$  (4.10) and the coefficient matrix  $c_{i\beta}$  (4.6) of the  $\beta$ th linearly independent solution of the Schrödinger equation in the volume  $V$ .

While the eigenvalue system for  $b_\beta$ , Eq. (4.7), can be solved directly, a more efficient approach is to partition the matrices  $\underline{\Gamma}$  and  $\underline{\Lambda}$  into open and closed subspaces [68]. The open subspace, denoted by a subscript “o,” consists of the few ( $N_o$ ) basis functions that are nonzero on the surface at  $r_0$ . The remaining  $N_c = N - N_o$  basis functions, denoted by the subscript “c”, are zero on this boundary and make up the closed subspace. In this partitioned notation, the eigensystem, Eq. (4.7), becomes,

$$\begin{pmatrix} \underline{\Gamma}_{cc} & \underline{\Gamma}_{co} \\ \underline{\Gamma}_{oc} & \underline{\Gamma}_{oo} \end{pmatrix} \begin{pmatrix} \vec{c}_{c\beta} \\ \vec{c}_{o\beta} \end{pmatrix} = b_\beta \begin{pmatrix} 0 & 0 \\ 0 & \underline{\Lambda}_{oo} \end{pmatrix} \begin{pmatrix} \vec{c}_{c\beta} \\ \vec{c}_{o\beta} \end{pmatrix}. \quad (4.11)$$

This leads to a small eigensystem in the open subspace for the logarithmic derivative  $b$ ,

$$\underline{\Omega}_{oo} \vec{c}_{o\beta} = b_\beta \underline{\Lambda}_{oo} \vec{c}_{o\beta}, \quad (4.12)$$

where the matrix  $\underline{\Omega}_{oo} = \underline{\Gamma}_{oo} - \underline{\Gamma}_{oc} \underline{\Gamma}_{cc}^{-1} \underline{\Gamma}_{co}$  requires a calculation of the inverse  $\underline{\Gamma}_{cc}^{-1}$  in the larger closed subspace. The computational advantage of this partitioned notation is that the product  $\underline{X}_{cc} = \underline{\Gamma}_{cc}^{-1} \underline{\Gamma}_{co}$  can be found as the solution of the linear system,

$$\underline{\Gamma}_{cc} \underline{X}_{cc} = \underline{\Gamma}_{co}. \quad (4.13)$$

All of these results are standard formulas in variational  $R$ -matrix theory. The only modification that my calculations require is that the matrix  $\underline{\Gamma}$ , defined in Eq. (4.8) and used in Eqs. (4.11-4.13), is evaluated at complex energies  $E + i\Gamma/2$ , so that the final eigenvectors  $\vec{c}_\beta$  and logarithmic derivatives  $b_\beta$  are complex.

An important technical detail in solving the  $R$ -matrix equations is the choice of an appropriate set of basis functions  $y_i(\vec{x})$ . To calculate the long-range  $S$ -matrix  $\underline{S}^{\text{LR}}$ , I use  $L$  spherical harmonics  $Y_{lm}(\theta, \phi)$  for the angular degrees of freedom and  $P$  basis splines  $B_p(r)$  [118] for the radial degree of freedom:

$$y_i(\vec{x}) = Y_{lm}(\theta, \phi)B_p(r),$$

$$l = \{0, 2, \dots, 2L - 2\} \quad (\text{even parity}),$$

$$l = \{1, 3, \dots, 2L - 1\} \quad (\text{odd parity}),$$

$$p = \{1, \dots, P\},$$

$$i = \{l, m, p\} = \{1, \dots, N = LP\}.$$

Only one value of  $m$  is present in the expansion of the wavefunction because the Hamiltonian, Eq. (4.1), is symmetric under rotations about the  $z$ -axis. And, because spin-orbit and hyperfine effects are neglected, the Hamiltonian (4.1) is invariant under the parity operation  $z \rightarrow -z$  so that only odd or else only even parity spherical harmonics are needed. The spherical harmonics are convenient because they also serve as channel functions on the sphere at  $r = r_0$ , where the physics is purely Coulombic.

The basis (or B) splines are a convenient set of locally defined functions that can represent the radial part of the wavefunction. Here, only their properties that are relevant for solving the Schrödinger equation for the case at hand are presented. The reader is referred to the text of de Boor [118] for a formal discussion of their many mathematical properties. Examples of their use in atomic physics can be found in the article of Sapirstein and Johnson [119]. For the radial wavefunction, a set of  $P$  B-splines of order  $k$  is used. These splines, which are polynomials of order  $k$  locally, are defined on a radial mesh of  $N_r$  points on the interval  $[r_0, r_{max}]$ . Given the number of mesh points  $N_r$  and the order of spline  $k$ , the number of splines is constrained to be  $P = N_r + k - 1$ . The details of the splines are determined by how the set of mesh points is chosen. I use a convention where the mesh points at the limits of the interval

are repeated  $k$  times. With this choice, there is a single spline nonzero at each boundary ( $B_1(r_0) = 1$  and  $B_P(r_{max}) = 1$ ), and all others are zero at  $r_0$  and  $r_{max}$ . The advantage of choosing the splines in this manner is that the boundary conditions on the wavefunction at  $r_0$  and  $r_{max}$  can be imposed without difficulty. Below threshold, the wavefunction must vanish at the outer radius  $r_{max}$ . This is accomplished by excluding the last spline  $B_P$  from the expansion of the wavefunction. At the inner boundary  $r_0$  there are two possibilities. For channels in the closed subspace, the wavefunction is zero on the surface  $r = r_0$  so that the nonzero spline  $B_1$  is again excluded for these channels. However, in the open channels, this spline must be kept to represent finite values of the logarithmic derivatives  $b_\beta$  on the surface.

This choice of basis functions leads to an efficient method of solving the large linear system, Eq. (4.13), and the smaller eigensystem, Eq. (4.12), of  $R$ -matrix theory. This is the case because the spherical harmonics and B-splines lead to a highly banded matrix structure for the large matrix  $\underline{\Gamma}_{cc}$ . The only term in the Hamiltonian that is nondiagonal in the spherical harmonic basis is the diamagnetic term  $\frac{1}{8}B^2r^2\sin^2\theta$ , which couples angular momentum  $l$  to  $l \pm 2$ . The angular matrix elements of the diamagnetic term can be worked out analytically in terms of the  $6j$  coefficients [120]:

$$\langle lm | \sin^2 \theta | l' m \rangle = \frac{2}{3} \left( \delta_{ll'} - (-1)^m \sqrt{(2l+1)(2l'+1)} \begin{Bmatrix} l & l' & 2 \\ 0 & 0 & 0 \end{Bmatrix} \begin{Bmatrix} l & l' & 2 \\ -m & m & 0 \end{Bmatrix} \right).$$

The radial matrix elements in  $\underline{\Gamma}$  (4.8) and  $\underline{\Delta}$  (4.9) involve integrals over the B-splines and their derivatives. These matrix elements are calculated numerically using Gaussian quadrature. The values of the B-splines and their derivative needed for the integrals can be generated rapidly using the Fortran routines listed in the text of de Boor [118]. Most importantly, for  $k$ th order splines, each spline overlaps with only  $k - 1$  other splines. These properties of the spherical harmonics and B-splines lead to a matrix  $\underline{\Gamma}_{cc}$  with a total bandwidth of  $4P + 2k - 9$ . Thus, even though the matrix  $\underline{\Gamma}_{cc}$  is of order  $L \times P$ , the linear system involving this matrix, Eq. (4.13), can be solved efficiently using the banded matrix routines found in the LAPACK Fortran library [121].

In numerical tests I have found that for an electron at energy  $E = -1/2\nu^2$  using  $\nu/2$  spherical harmonics of a given parity ( $L = \nu/2$ ) and  $4\nu$  B-splines ( $P = 4\nu$ ) gives about 4 digits of accuracy in the long-range  $S$ -matrix. Almost always, B-splines of order  $k = 5$  are sufficient. These guidelines

for picking the number of basis functions (and the order of splines) leads to a closed subspace of order  $N_c \approx 2\nu^2$  and a total bandwidth of  $16\nu + 2k - 9$  for the matrix  $\underline{\Gamma}_{cc}$ . As an example, for  $\nu = 50$ , the solution of the large linear system, Eq. (4.13), at each energy takes  $\approx 30$  seconds of CPU time and  $\approx 150$  Mb of memory on a 633 Mhz Compaq Alpha workstation. Because the open subspace is typically of order  $N_o \approx 5 - 10$ , the small eigenvalue problem, Eq. (4.12), takes only a fraction of a second. Next I describe how the long-range  $S$ -matrix  $\underline{S}^{\text{LR}}$  can be found, once the  $R$ -matrix equations have been solved to give  $b_\beta$  and  $c_{i\beta}$ .

#### 4.1.2 Finding the $S$ -matrix

Solution of the  $R$ -matrix equations above constitutes the main computational work involved in calculating the long-range  $S$ -matrix. Once these calculations have been performed, the multichannel radial wavefunction  $F_{i\beta}(r)$  on the surface  $r = r_0$  takes the simple form:

$$F_{i\beta}(r_0) = c_{i\beta}. \quad (4.14)$$

Furthermore, this form of the wavefunction (4.14), along with the definition of the logarithmic derivative  $-b_\beta$  (4.10) yields the radial derivative of the wavefunction on the boundary:

$$\frac{\partial F_{i\beta}(r_0)}{\partial r} = c_{i\beta} b_\beta, \quad (4.15)$$

where one must take into account that  $\hat{n} = -\hat{r}$  on the surface  $r = r_0$  to get this result. As described in Ch. 2,  $\underline{S}^{\text{LR}}$  emerges when this numerically determined solution is matched to the  $S$ -matrix state, Eq. (2.18):

$$\underline{M}^{\text{LR}}(r) = \frac{1}{i\sqrt{2}} [\underline{f}^-(r)\underline{S}^{\text{LR}} - \underline{f}^+(r)]. \quad (4.16)$$

In the matching region, where the electron moves in a pure Coulomb potential, the numerical wavefunction, Eq. (4.14), can be written in terms of the Coulomb functions  $(f_i^+, f_i^-)$  and constant coefficient matrices  $\underline{P}$  and  $\underline{Q}$  (see Eq. (4.17)):

$$F_{i\beta}(r_0) = c_{i\beta} = \frac{1}{i\sqrt{2}} [f_i^+(r_0)P_{i\beta} - f_i^-(r_0)Q_{i\beta}]. \quad (4.17)$$

Taking the Wronskian of this wavefunction (4.17) with  $f_i^+(r)$  and  $f_i^-(r)$  gives the coefficient matrices  $\underline{P}$  and  $\underline{Q}$  in terms of the  $R$ -matrix solution matrix  $c_{i\beta}$ :

$$P_{i\beta} = \frac{\pi}{\sqrt{2}} \mathbf{W} [f_i^+, c_{i\beta}]_{r_0} = \frac{\pi}{\sqrt{2}} (f_i^+(r_0)b_{i\beta} - f_i^{+\prime}(r_0)) c_{i\beta}, \quad (4.18)$$

$$Q_{i\beta} = \frac{\pi}{\sqrt{2}} \mathbf{W} [f_i^-, c_{i\beta}]_{r_0} = \frac{\pi}{\sqrt{2}} (f_i^-(r_0)b_{i\beta} - f_i^{-\prime}(r_0)) c_{i\beta}. \quad (4.19)$$

Finally, the long-range  $S$ -matrix can be written in terms of these numerical coefficients, Eqs. (4.18) and (4.19):

$$\underline{S}^{\text{LR}} = \underline{P}\underline{Q}^{-1}. \quad (4.20)$$

I emphasize that all of the quantities in the above discussion ( $b_{i\beta}$ ,  $c_{i\beta}$ ,  $P_{i\beta}$  and  $Q_{i\beta}$ ) are strongly varying functions of both the magnetic field  $B$  and the complex valued energy  $E + i\Gamma/2$ . Thus, this entire procedure must be repeated at each energy. In principle, the Coulomb functions ( $f_l^+$ ,  $f_l^-$ ) and their derivatives in Eqs. (4.18) and (4.19) must also be evaluated at complex energies. However, at the moderate distances in the matching region ( $10 < r_0 < 100$ ) the Coulomb functions at complex energies can be approximated by their values on the real energy axis without any sacrifice in the accuracy in the final  $S$ -matrix, Eq. (4.20). A justification of this approximation is given in Fig. 4.2, which plots the regular and irregular Coulomb functions at a complex energy typical of what is required for the preconvolution of the  $S$ -matrix and cross section. The upper graph shows the imaginary parts of ( $f$ ,  $g$ ), which vanish at real energies. Because these imaginary parts are orders of magnitude smaller than the real parts the Coulomb functions  $f^\pm = (-g \pm if)/\sqrt{2}$  in the matching region can be calculated on the real energy axis. However, if the complex energy Coulomb functions are needed, they can be calculated with formulas given by Robicheaux [105].

One final detail about the numerically calculated  $\underline{S}^{\text{LR}}$  needs to be addressed. A certain amount of flexibility exists in how the dimensionality of  $\underline{S}^{\text{LR}}$  is chosen. When  $\underline{S}^{\text{LR}}$  is initially calculated, it must include all of the channels that are locally open (classically allowed) and weakly closed on the surface at  $r = r_0$ . This number of channels  $N_o$  determines the size of the open subspace in the  $R$ -matrix calculations and is typically a few more than the maximum classical allowed angular momentum  $l_{max}$

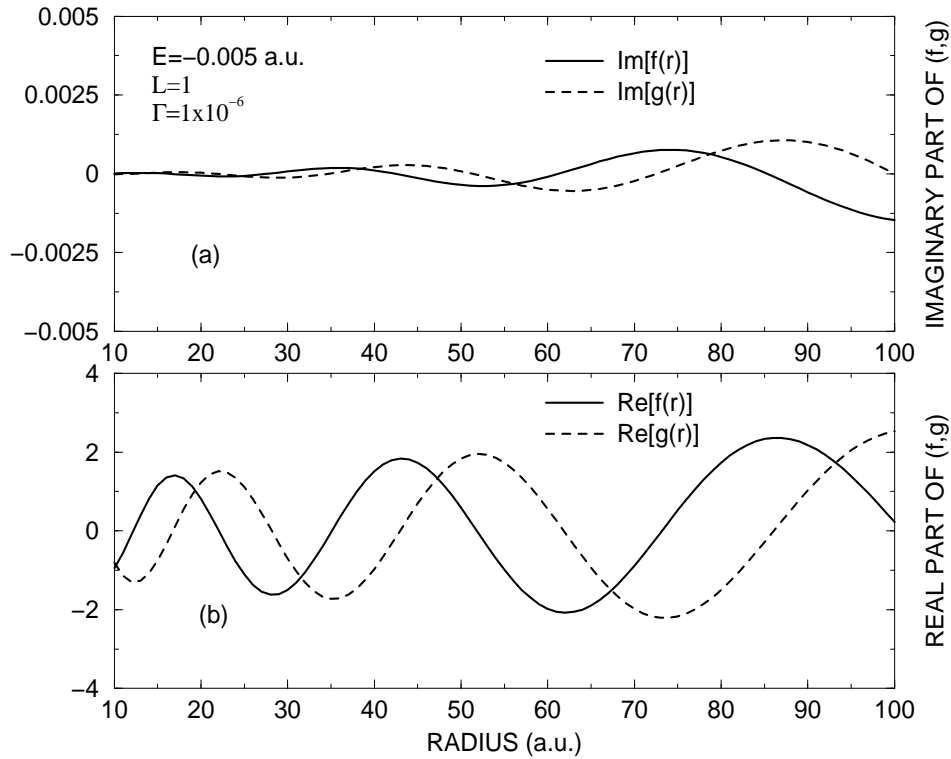


Figure 4.2: The real (bottom) and imaginary (top) parts of the regular (solid line) and irregular (dotted line) Coulomb functions ( $f, g$ ) are plotted at a complex energy  $E = -0.0005 + 0.5 \times 10^{-6}i$  and angular momentum  $l = 1$ . On the real energy axis, these two Coulomb functions are real-valued. This figure shows that when the energy is complex, these Coulomb functions develop small imaginary parts that increase with the radius  $r$ . The traveling wave Coulomb functions used in Eqs. (4.18) and (4.19) to find the long-range  $S$ -matrix are related to these functions through the relation  $f^\pm = (-g \pm if)/\sqrt{2}$ . Technically, the complex energy Coulomb functions shown in this figure should be used (through  $f^\pm$ ) to find the preconvoluted  $S$ -matrix  $\underline{S}^{\text{LR}}$ . However, because the imaginary parts of  $(f, g)$  are orders of magnitude smaller than the real parts, it is a good approximation to use the Coulomb functions at real energies. It is important to note that this approximation is only good at small radii; as  $r$  is increased, the imaginary parts of  $f$  and  $g$  eventually overtake the real parts. Thus, by keeping the matching radius small ( $r_0 \approx 10$  a.u.), the complications of calculating the Coulomb functions at complex energies can be avoided.

on the matching surface:

$$l_{\max} = \sqrt{2r_0^2 \left( E + \frac{1}{r_0} \right)} - \frac{1}{2}. \quad (4.21)$$

However, all of these  $N_o \approx l_{\max}$  channels are not needed explicitly in the formula for the photoabsorption cross section, Eq. (3.28). This is because the short range parameters  $\vec{d}$  and  $\underline{S}^{\text{core}}$  used in the cross section are typically trivial (0 or 1) beyond the first few channels. For example, in Li the quantum defects are  $\mu_s = 0.4$  and  $\mu_p = 0.04$ ; all others are smaller than 0.01. As Harmin [83] has shown, the “extra” channels in  $\underline{S}^{\text{LR}}$  can be eliminated using the tools of quantum-defect theory. This is desirable because the wavefunction in these weakly closed channels becomes exponentially large at small distances. Labeling the unwanted channels by the subscript “x” (for extra) and those to be maintained by the subscript “p” (for physical),  $\underline{S}^{\text{LR}}$  can be written in a partitioned notation,

$$\underline{S}^{\text{LR}} = \begin{pmatrix} \underline{S}_{pp}^{\text{LR}} & \underline{S}_{px}^{\text{LR}} \\ \underline{S}_{xp}^{\text{LR}} & \underline{S}_{xx}^{\text{LR}} \end{pmatrix}, \quad (4.22)$$

where the total dimension of  $\underline{S}^{\text{LR}}$  is  $N_o = N_p + N_x$ . The physical long-range  $S$ -matrix  $\underline{S}^{\text{LR,phys}}$  having dimension  $N_p$  can be found in terms of the partitions of the raw  $S$ -matrix, Eq. (4.23):

$$\underline{S}^{\text{LR,phys}} = \underline{S}_{pp}^{\text{LR}} + \underline{S}_{px}^{\text{LR}} (\underline{1} - \underline{S}_{xx}^{\text{LR}})^{-1} \underline{S}_{xp}^{\text{LR}}. \quad (4.23)$$

The advantage of using this smaller  $S$ -matrix  $\underline{S}^{\text{LR,phys}}$  is that it shows a weaker dependence on the matching radius  $r_0$  than the raw  $S$ -matrix  $\underline{S}^{\text{LR}}$ . It is important, however, to note that both  $\underline{S}^{\text{LR,phys}}$  and  $\underline{S}^{\text{LR}}$  give identical photoabsorption cross sections when used in Eq. (3.28). In addition, while both these  $S$ -matrices depend weakly on  $r_0$ , the total photoabsorption cross section is found to be independent of  $r_0$ . It is often useful to study the long-range  $S$ -matrix directly rather than the total photoabsorption cross section. When this type of analysis is performed, it is more sensible to use  $\underline{S}^{\text{LR,phys}}$  which is nearly independent of the radius  $r_0$ . In fact, for the remainder of this thesis, I will always use  $\underline{S}^{\text{LR,phys}}$  when an accurate quantum  $S$ -matrix is needed; the superscript “phys” will subsequently be dropped.

### 4.1.3 Scaled variable $S$ -matrices

This section has described a method for calculating the long-range  $S$ -matrix for the motion of an atomic electron at energy  $E$  in a static magnetic field of strength  $B$ . In most cases, however, it is more useful to study the physics of such an electron using the scaled variables discussed in the Introduction and Appendix A. In this approach, the cross section and  $S$ -matrices are studied at a fixed scaled energy  $\epsilon = EB^{-2/3}$  as a function of the scaled magnetic field  $w = 2\pi B^{-1/3}$ . A simple variable transformation of the numerically calculated  $\underline{S}^{\text{LR}}(E, B)$  gives the needed scaled variable  $S$ -matrix  $\underline{S}^{\text{LR}}(\epsilon, w)$ :

$$\underline{S}^{\text{LR}}(\epsilon, w) = \underline{S}^{\text{LR}}(E(\epsilon, w), B(\epsilon, w)), \quad (4.24)$$

$$E(\epsilon, w) = \epsilon \left( \frac{2\pi}{w} \right)^2 \left( 1 - i2 \frac{\Delta w}{w} \right), \quad (4.25)$$

$$B(\epsilon, w) = \left( \frac{2\pi}{w} \right)^3. \quad (4.26)$$

This rescaling generates a cross section  $\sigma^{\Delta w}(\epsilon, w)$  and  $S$ -matrix  $\underline{S}^{\text{LR}}(\epsilon, w)$  in the  $w$  domain that has been preconvolved with a Lorentzian of width  $\Delta w$ . I emphasize that unlike other quantum mechanical methods [75] of calculating the scaled photoabsorption cross section, no recasting of the Schrödinger equation is needed in my approach; the energy and magnetic field of Eqs. (4.25) and (4.26) are simply used in the  $R$ -matrix calculations described above.

## 4.2 Recurrences in the quantum $S$ -matrix

My choice of using scattering matrices to describe the motion of an atomic electron in an external magnetic field is based on two important points. First, the  $S$ -matrices  $\underline{S}^{\text{LR}}$  and  $\underline{S}^{\text{core}}$  contain all of the important physics of the electron. Second, after they have been calculated, these  $S$ -matrices can be used to gain physical insight about the electron's motion. In this chapter, the necessary details for calculating the long-range  $S$ -matrix  $\underline{S}^{\text{LR}}(\epsilon, w)$  have been given for an atom in a static external magnetic field. In this final section, calculations of  $\underline{S}^{\text{LR}}(w)$  are presented that implement this approach.

The calculations presented here are given in terms of the scaled variables of Appendix A. Thus, the scattering matrix  $\underline{S}^{\text{LR}}(w)$  has been calculated at a fixed scaled energy  $\epsilon$  as a function of the “energy”-

like scaled variable  $w$ . In the spirit of closed-orbit theory, these accurate quantum  $S$ -matrices are then Fourier transformed into the scaled action domain. The information contained in the Fourier transform of the matrix element  $S_{ll'}^{\text{LR}}(w)$  is best presented in terms of the recurrence strength  $R(\tilde{S})$ . I define the recurrence strength  $R(\tilde{S})$  of some  $w$ -domain function  $f(w)$  in the interval  $[w_1, w_2]$  as the windowed Fourier transform:

$$R(\tilde{S}) = \left| \int_{w_1}^{w_2} f(w) e^{-i\tilde{S}w} e^{-(w-w_0)^2/(2\delta)} dw \right|, \quad (4.27)$$

where  $\delta = (w_1 + w_2)/6$  and  $w_0 = (w_1 + w_2)/2$ . The windowing function  $\exp(-(w - w_0)^2/(2\delta))$  is used to eliminate artificial side peaks in the recurrence strength. Note that my definition of  $R(\tilde{S})$  involves the absolute value of the Fourier transform rather than absolute value squared as some researchers use. This choice accentuates smaller features in the recurrence strength that are diminished when the result of the Fourier transformation in Eq. (4.27) is squared.

First, calculations of the long-range  $S$ -matrix  $\underline{S}^{\text{LR}}(w)$  at a scaled energy of  $\epsilon = -0.7$  are presented. At this scaled energy, the classical dynamics are mostly regular (see Fig A.1, Appendix A). This results in relatively few quantum paths contributing to the long-range  $S$ -matrix. By plotting the elements of  $\underline{S}^{\text{LR}}$  in both the  $w$  domain (Fig. 4.3) and in the Fourier domain (Fig. 4.4) the most important quantum mechanical paths of the electron can be “seen.” First, Fig. 4.3 shows the real part of the matrix element  $S_{00}^{\text{LR}}(w)$  as a function of the scaled field  $w$ . This matrix element shows oscillations with  $w$ , indicating that a few features in the scaled action domain are controlling the long-range  $S$ -matrix. The calculations presented in Fig. 4.4 confirm the presence of the short action contributions to the  $S$ -matrix. Here, the Fourier transforms (recurrence strengths) of the quantities  $\text{Re}(S_{00}^{\text{LR}}(w))$ ,  $\text{Re}(S_{22}^{\text{LR}}(w))$  and  $\text{Re}(S_{44}^{\text{LR}}(w))$  over the range  $w = 100 - 500$  are shown. All of these matrix elements show strong recurrences at the same scaled actions. This shows that the same quantum amplitudes contribute to each element of  $\underline{S}^{\text{LR}}$  at a given scaled energy. Of course at this point, without borrowing the insights of closed orbit theory, it would difficult to understand exactly to what the recurrences in the matrix  $\underline{S}^{\text{LR}}$  correspond. The important point of these accurate quantum calculations is that the physics of the long-range  $S$ -matrix is controlled by a few features in the scaled action domain. The most that can be said without invoking

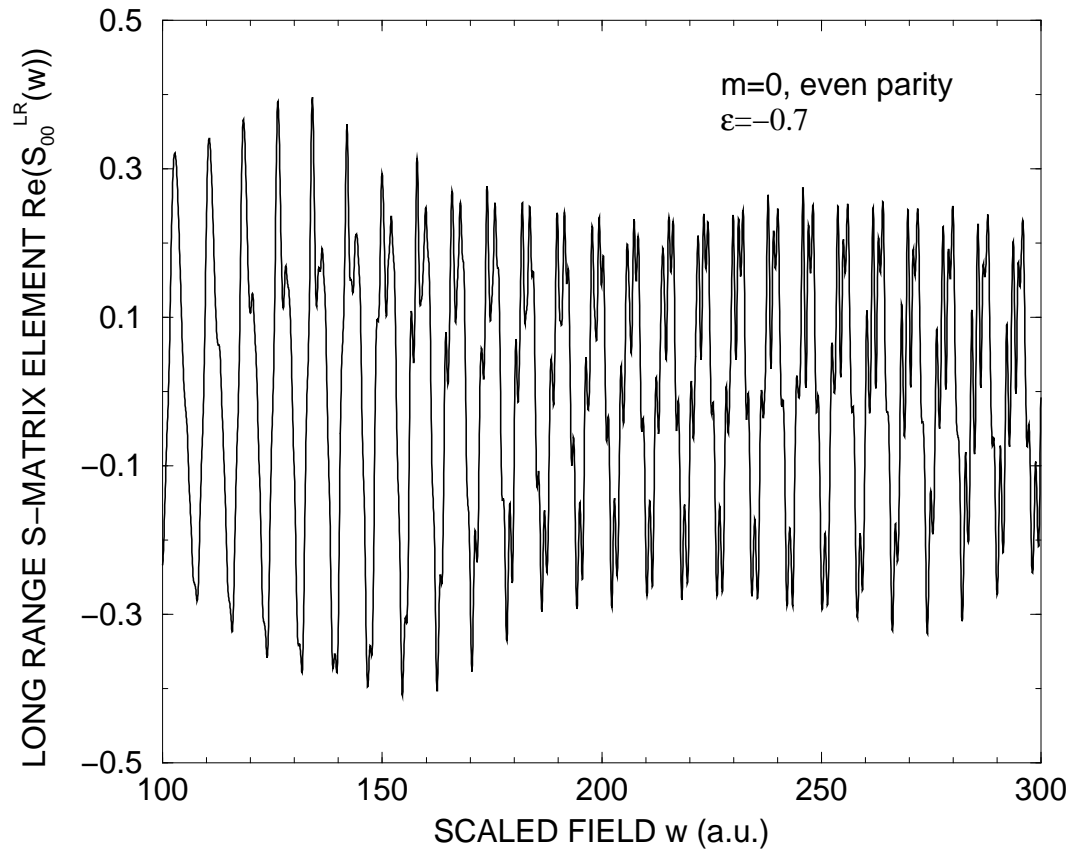


Figure 4.3: The real part of an element of  $\underline{S}^{\text{LR}}$  is shown as a function of the scaled field  $w$ . Here, a low angular momentum piece  $\text{Re}(S_{00}^{\text{LR}}(w))$  of the long range  $S$ -matrix is plotted at a scaled energy of  $\epsilon = -0.7$ , where the classical motion is mostly regular. This matrix element, and the others in  $\underline{S}^{\text{LR}}$ , provide a complete description of the electron's motion as it scatters off the long-range Coulomb and diamagnetic potential. This matrix element was calculated using the variational  $R$ -matrix method of this chapter, and has been preconvolved with a width  $\Delta w = 0.5$  in the  $w$  domain. The most important feature of this figure is that the matrix element oscillates with  $w$ . High frequency oscillations have been smoothed out with the preconvolution technique, leaving only the largest scale oscillations visible. As a Fourier transform of this matrix element shows (see Fig. 4.4, panel (c)), these oscillations are due to a few quantum mechanical paths of the electron having short scaled actions. The  $S$ -matrix shown here is for an  $m = 0$ , even parity electron.

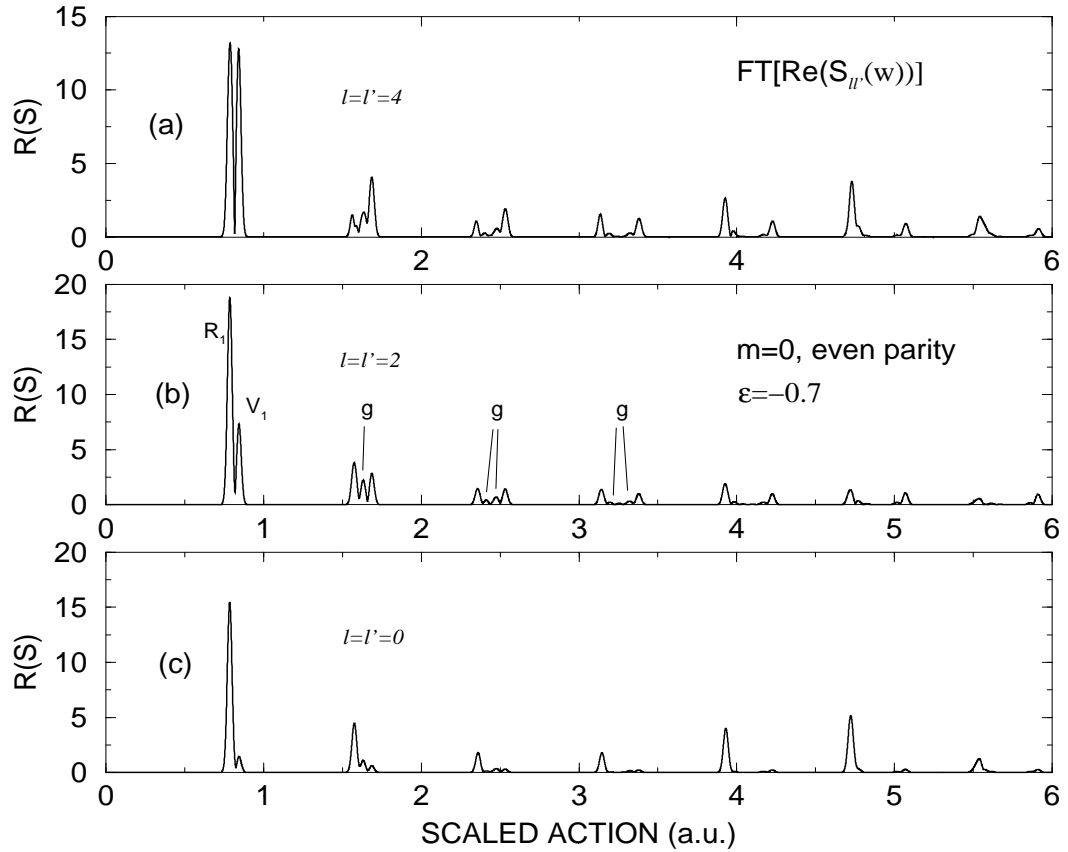


Figure 4.4: The Fourier transforms or recurrence strengths ( $R(\tilde{S})$ , Eq. (4.27)) of individual elements of the long range  $S$ -matrix are shown. As in Fig. 4.3, a scaled energy of  $\epsilon = -0.7$  is used here. The recurrence strength of the matrix element plotted in Fig. 4.3 ( $Re(S_{00}^{LR}(w))$ ) is shown in the lower panel (c). The middle panel (b) and upper panel (a) give the recurrence strength for higher angular momentum elements ( $Re(S_{44}^{LR}(w))$  and  $Re(S_{22}^{LR}(w))$  respectively) of the same long range  $S$ -matrix. All three matrix elements exhibit the same sharp peaks in the scaled action domain, with only the amplitudes varying with the angular momentum. The semiclassical methods of the following chapter correlate most of these recurrence peaks with classical closed orbits of the electron. For instance, the shortest action recurrence peak in this graph, labeled  $R_1$ , corresponds to the quasi-Landau orbit observed in the first experiments by Garton and Tomkins [27]. The next longest action peak ( $V_1$ ) is correlated with the electron's motion parallel to the magnetic field. The contributions of harmonics, or repetitions, of these two short action paths are also seen. Because these are recurrence strengths of an accurate quantum  $S$ -matrix, some of the recurrence peaks are nonclassical. More specifically, the peaks labeled with the letter "g" - for ghost - have no radially returning classical closed orbits associated with them. Again, the  $S$ -matrix shown is for an  $m = 0$ , even parity electron.

the ideas of closed-orbit theory is this: because the  $S$ -matrix elements are quantum mechanical amplitudes for the electron to scatter off the long-range potential, the recurrence peaks in the elements of  $\underline{S}^{\text{LR}}$  correspond to different quantum mechanical paths that the electron has taken in its scattering process. The semiclassical approximations of the following chapter (Ch. 5) will link these quantum paths to the chaotic classical closed orbits of the electron.

It is also interesting to see how the recurrence structures in the long-range  $S$ -matrix evolve with the scaled energy  $\epsilon$ . In the classical motion of the electron, this parameter controls whether the dynamics are regular ( $\epsilon < -0.9$ ) or chaotic ( $\epsilon \rightarrow 0$ ). Figure 4.5 shows the recurrence strength of the quantity  $Re(S_{44}^{\text{LR}}(w))$  at seven scaled energies ranging from  $\epsilon = -0.9 \rightarrow -0.3$ . At the lower scaled energies, the recurrence strength is dominated by two short action quantum paths (labeled  $R_1$  and  $V_1$  after the closed orbits they represent) and their harmonics. As the scaled energy increases, additional recurrence peaks appear. This proliferation of recurrence peaks is one of the manifestations of the underlying classical chaos.

One of the main advantages of having accurate quantum scattering matrices to analyze is that nonclassical paths can be detected and studied. A recurrence peak is nonclassical if there is no classical closed orbit available to explain the recurrence. In the literature, these nonclassical features in the recurrence strength are often called ghost orbits. The most common place to see their presence is just below the scaled energies where new closed orbits bifurcate. Then, the ghost orbits can be viewed as the electron tunneling into an almost allowed classical trajectory. In both Figs. 4.4 and 4.5, I have marked the nonclassical features with the letter “g” - for ghost. Of course, the only way to distinguish between a real orbit and a ghost orbit is to perform a search for classical closed orbits. The results of such a search is given in Appendix B for scaled energies from  $\epsilon = -0.4 \rightarrow 0.0$ . After the classical search has been completed, any recurrence peaks in the quantum  $S$ -matrix  $\underline{S}^{\text{LR}}$  having no corresponding closed orbit can be labeled as a ghost orbit.

This chapter has shown that it is possible to calculate and study accurate long-range  $S$ -matrices  $\underline{S}^{\text{LR}}$  for the motion of an atomic electron in an external magnetic field. While the techniques for calculating this  $S$ -matrix are familiar tools of atomic theory, the use of complex energies to accomplish a

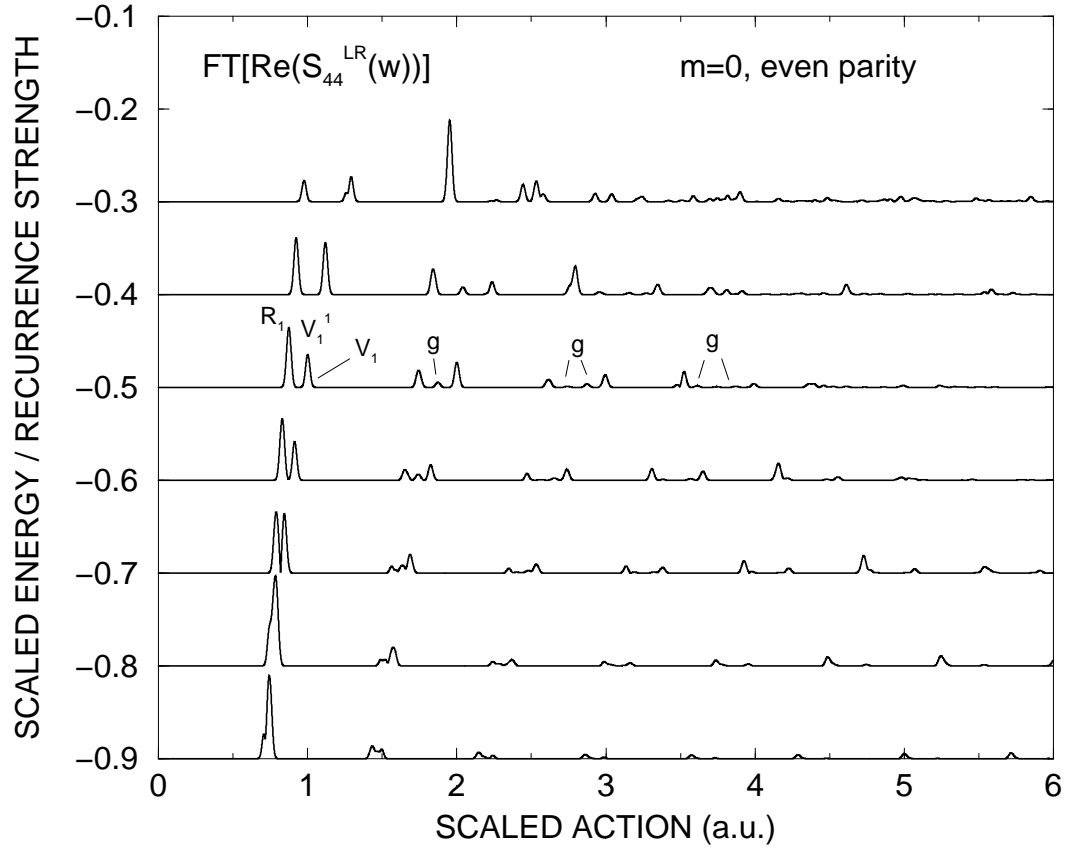


Figure 4.5: Recurrence strengths of the matrix element  $Re(S_{44}^{LR}(w))$  are plotted for multiple scaled energies. This shows how the recurrence peaks (each associated with one quantum path) evolve as the classical dynamics of the electron make a transition from being regular ( $\epsilon = -0.9$ ) to chaotic ( $\epsilon = -0.3$ ). Although the recurrence strength shown here is from an accurate variational  $R$ -matrix quantum calculation, the signatures of the underlying classical chaos can be seen in the increased number of recurrence peaks at higher scaled energies. Semiclassical approximations correlate most of the recurrence peaks in this figure with classical closed orbits of the electron. The three shortest action peaks are labeled with the closed orbit to which they correspond. Appendix B gives information about these closed orbits. Nonclassical recurrence peaks that are not related to any closed orbit are marked with the letter “g” - for ghost. The numbers on the vertical axis give the values of the scaled energy for each scan. The recurrence strengths have been scaled to allow multiple scaled energies to be shown on the same graph.

preconvolution of the  $S$ -matrix is novel. In addition, using scaled variables along with ideas from closed-orbit theory, the recurrences in the long-range  $S$ -matrix can be studied. This analysis allows the detection of nonclassical, or ghost, orbits that contribute to the long range physics. In Ch. 6, it will be seen that these ghost orbits play a critical role in the semiclassical photoabsorption cross section. I emphasize that in previous quantum calculations, only the recurrences of total photoabsorption cross section have been studied. My formula for the photoabsorption cross section shows that the cross section is complicated by multiple scatterings of the electron off the long-range and core regions. Being able to directly study the long-range  $S$ -matrix allows recurrences to be studied without the complications of the multiple scattering event that make up the cross section. The full interpretation of the recurrences, however, relies on the introduction of semiclassical approximations to the long-range  $S$ -matrix. The next chapter develops such approximations again, for an atomic electron in an external magnetic field.